

DOI: 10.1002/adma.200701063

Noncovalent Deposition of Nanoporous Ni Membranes on Spatially Organized Poly(*p*-xylylene) Film Templates**

By Melik C. Demirel,* Murat Cetinkaya, Alok Singh, and Walter J. Dressick*

Nickel metal is widely used in catalytic,^[1,2] energy storage,^[3,4] and optical applications^[5,6] due to its favorable physicochemical properties. Although Ni morphology, topology, and surface chemistry are critically important for these applications, their control is limited by: 1) Ni deposition conditions and treatments,^[7–9] and 2) properties and available architectures of sacrificial metallization templates,^[1,6,10–13] which are usually removed by (thermo)chemical treatments after plating. In this regard, we have been exploring poly(*p*-xylylene) nanostructured thin films (NTFs) formed through vapor-phase polymerization and directed deposition of [2.2]paracyclophane derivatives^[14,15] (Fig. 1A) as new metallization templates. Proper selection of the deposition geometry and conditions and the [2.2]paracyclophane derivative permits exquisite, simultaneous control of film morphology, topology, and surface chemistry, yielding NTFs with diverse, well-organized porous structures (Fig. 1B–C). Here, we present our initial results relating to the fabrication and characterization of nanoporous Ni membranes templated by conformal electroless (EL) metallization of poly(chloro-*p*-xylylene) (PPX-C) NTFs.

EL metallization of polymer films is typically a multistep process^[16] involving: 1) chemical or mechanical surface micro-roughening to promote metal adhesion; 2) adsorption of Pd/Sn core/shell colloids to the surface; 3) selective dissolution of the Sn^{II/IV} β -hydroxy shell segment *not* anchoring the colloid to the surface to expose the catalytic Pd⁰ core; and finally 4) solution deposition of EL metal. For NTFs, however, the need to minimize potential damage to film nanoarchitectures (Fig. 1), eliminate environmentally hazardous Sn salts, and reduce process steps and costs necessitates consideration of an alternate EL plating procedure. In one

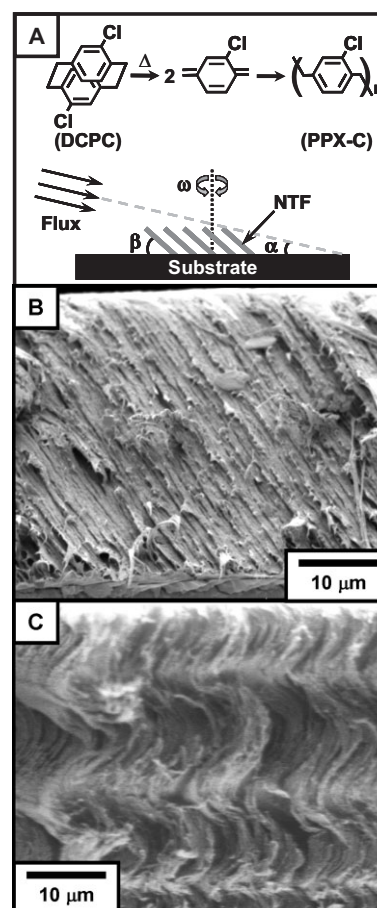


Figure 1. A) Pyrolysis reaction for formation of poly(chloro-*p*-xylylene) (PPX-C) from dichloro-[2.2]paracyclophane (DCPC) with schematic for fabrication of NTFs (note Experimental Section); B) SEM cross-section of columnar PPX-C NTF on Si wafer ($\alpha = 10^\circ$, $\beta = 55^\circ$, $\omega = 0 \text{ s}^{-1}$); C) SEM cross-section of right-handed PPX-C NTF helices on Si wafer ($\alpha = 10^\circ$, $\beta = 90^\circ$, $\omega = 0.167 \text{ s}^{-1}$). The morphology of NTFs in parts (B) and (C) consisted of bundled polymer strands of ~ 50 – 200 nm strand diameter.

[*] Prof. M. C. Demirel, M. Cetinkaya
 Pennsylvania State University
 University Park, PA 16802 (USA)
 E-mail: mdemirel@engr.psu.edu
 Dr. W. J. Dressick, Dr. A. Singh
 Naval Research Laboratory
 Code 6900, 4555 Overlook Avenue, S.W.
 Washington, DC 20375 (USA)
 E-mail: wjd@cbmse.nrl.navy.mil

[**] We gratefully acknowledge financial support for this work from the Pennsylvania State University and the Office of Naval Research under the Naval Research Laboratory Core 6.2 Research Program and the Young Investigator Program. Supporting Information is available online from Wiley InterScience or from the author.

such process,^[17–21] solvent-templated sites tailored to adsorb catalyst-binding pyridine ligands are first created at a polymer surface during film formation. Partitioning of pyridine from aqueous solution into these sites, driven by maximization of hydrophobic van der Waals and π - π interactions with the polymer aromatic functional groups that define the sites, non-covalently binds pyridine ligands at the polymer surface. Because the hydrophilic N site of the adsorbed pyridine remains accessible to aqueous solution, covalent binding of Pd^{II} EL

catalysts, in quantities exceeding the $\sim 10^{15}$ Pd^{II} ions cm⁻² threshold^[22] required for EL metal deposition, is facilitated.

For NTFs, however, the absence of solvent during vapor-phase deposition (Fig. 1A) precludes direct use of this metallization approach. Nevertheless, we reasoned that appropriate adsorption sites for pyridine ligands might be created during film vapor deposition due to the amorphous nature of the surface and the nanoscale PPX-C NTF dimensions (Fig. 1).^[14,15] Figure 2 is a schematic representation of our approach. In general, polymer chains comprising amorphous film surface regions can provide accessible pyridine adsorption sites through formation of noncovalent li-

bind sufficient Pd^{II} (step 2B) for sustained surface metallization (step 3B) and little or no Ni deposits ($\sim 0\text{--}5\%$ spotty Ni surface plating; not shown).

Experimental results support the differential ligand adsorption model of Figure 2. For example, thermally induced changes in polymer chain conformations continually create new surface sites capable of intercepting and binding additional ligand. Consequently, in time even a planar polymer film can adsorb sufficient pyridine to promote plating. In fact, surfaces of planar PPX-C films pyridine-treated for longer times (i.e., several days) are increasingly plated, consistent with our model. Further support for the process is obtained from surface analyses of helical NTFs following each treatment. For example, a strong X-ray photoelectron spectroscopy (XPS) Ni 2p signal observed at 852 eV identifies the material deposited on the NTF (Fig. 3A, inset) as Ni metal following completion of the process of Figure 2. Analysis of the Pd 3d_{5/2} XPS region for a sample treated sequentially with pyridine (aq) and PD1 Pd^{II} catalyst^[23] (note Experimental Section) *prior* to Ni deposition reveals a Pd^{II} signal (0.74 at %) with components at ~ 339 eV (Pd^{II}-N) and $\sim 337\text{--}338$ eV (Pd^{II}-Cl and Pd^{II}-O(H)) indicative of chloro/hydroxyl-bridged Pd^{II} colloids covalently bound to the pyridyl N sites (see Supporting Information Fig. S-1A).^[22,23]

Two additional points are worth noting with regard to PPX-C NTF surface treatments by PD1 catalyst and pyridine ligand. First, some direct adsorption of Pd^{II} to the NTF surface also occurs in the absence of adsorbed ligand, in agreement with earlier observations regarding PD1 catalyst interactions with high-energy surfaces.^[13,24] However, the quantity of Pd^{II} adsorbed (0.39 at %) is insufficient to promote Ni metallization, indicating that pyridine functions to sufficiently increase the local Pd^{II} surface concentrations to levels^[22] that catalyze Ni deposition. Second, we observe a weak XPS N 1s signal at 400 eV for a pyridine-treated NTF (Fig. S-1B), indicating that at least a portion of the pyridine resists outgassing from the NTF in the XPS high-vacuum chamber and is strongly adsorbed at the surface. Similar behavior has been noted for solvent-templated planar polymer films, where strong pyridine adsorption contributes to lithographic performance and improved adhesion of the EL Ni film.^[17,19] In fact, the EL Ni films deposited here on helical and columnar NTFs also exhibit good adhesion (< 5 % Ni delamination in “Scotch tape” tests), consistent with the behavior noted for solvent-templated planar polymer films. For NTFs, however, the tailored surface morphology and/or topology can provide an additional factor promoting Ni adhesion not available for corresponding solvent-templated planar polymer films.

The scanning electron microscopy (SEM) analysis in Figure 3A shows that Ni is deposited as a porous metal film on the underlying helical NTF. Similar topologies are observed by atomic force microscopy (AFM) for a helical NTF before and after Ni deposition (Fig. 3B–C). This is consistent with a conformal, templated Ni deposition process. Conformal Ni deposition is confirmed in Figure 3D, which shows the SEM cross section of a Ni-plated helical NTF prepared using

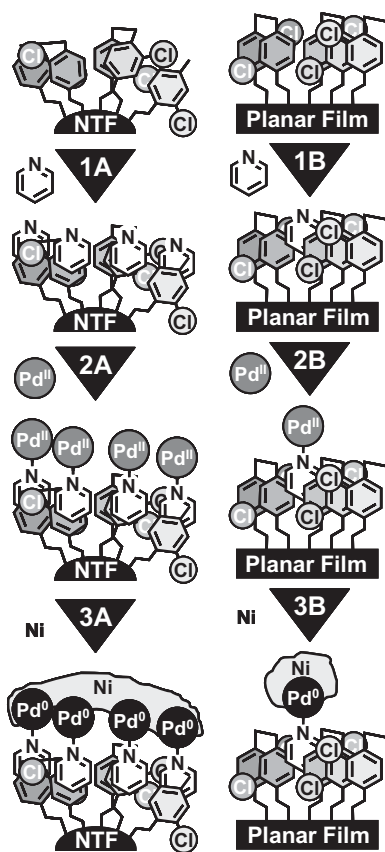


Figure 2. Scheme for electroless Ni film deposition onto Poly(*p*-xylylene) films. Process models are shown for nanostructured films (Path A) and planar films (Path B).

gand–polymer interactions.^[17,18] Enhanced surface disorder expected for higher surface energy (i.e., high curvature, approximately ~ 150 nm diameter) NTF polymer filaments^[14,15] provides a potential mechanism for more rapid adsorption of larger quantities of ligand relative to a planar PPX-C film (Fig. 2, steps 1A vs. 1B). Consequently, levels of adsorbed pyridine capable of covalently binding sufficient Pd^{II} (step 2A) to initiate EL Ni deposition (step 3A) can be achieved for the NTF, leading to confluent Ni plating (Fig. 3A, inset). In contrast, under identical treatment conditions (note Experimental Section) levels of adsorbed ligand at planar films cannot

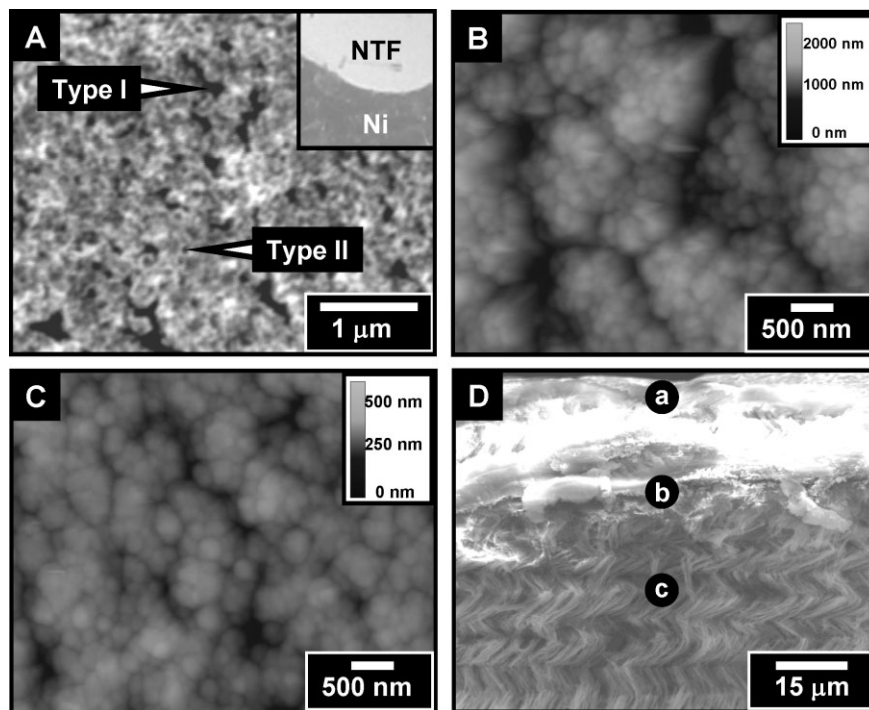


Figure 3. Film characterization. A) SEM of top surface of Ni film (light areas) on a helical NTF showing bimodal distribution of pores (dark areas). Examples of larger irregular Type I and smaller nearly circular Type II pores are highlighted. Inset: Low-resolution view of Ni plated helical NTF. Width of image is 1 cm; B) Typical contact mode AFM image of the top surface of an unmetallized helical PPX-C NTF; C) Representative contact mode AFM image of the top surface of a Ni plated helical PPX-C NTF. Image does not correspond to the same portion of the NTF as shown in part (B) above; D) SEM cross-section of Ni coated (upper light area) helical PPX-C NTF (lower gray area). Points “a” (Ni top surface), “b” (Ni–NTF interface, 20 μm depth), and “c” (nonplated NTF interior, 40 μm depth) mark the areas selected for EDAX analysis in Supporting Information Figure S-2.

a pyridine (aq) solution treatment. An energy-dispersive X-ray (EDAX) depth-profile analysis of the results shown in Figure 3D identifies the coating as Ni metal and indicates that it penetrates the NTF to a depth of $\sim 20 \mu\text{m}$ (Fig. S-2). It is interesting to note that analogous experiments using pyridine vapor led to deeper penetration of Ni ($\sim 40 \mu\text{m}$, not shown), permitting tuning of the Ni membrane thickness. Such behavior is consistent with the model in Figure 2 insofar as water, which solvates pyridine well but penetrates the hydrophobic pores of the NTF with difficulty, effectively limits the contact of the pyridine to adsorption sites nearer to the NTF surface. In contrast, hydrophobic pyridine molecules in the vapor phase are capable of deeper penetration into the NTF pores, rendering hydrophobic NTF pore surfaces sufficiently hydrophilic upon pyridine adsorption to facilitate deeper aqueous transport of the PD1 for catalysis and of the EL Ni bath for plating.

Table 1 summarizes the root mean square (RMS) surface roughness and surface porosity values obtained from the AFM measurements for Ni films deposited on planar, helical NTF, and columnar NTF PPX-C films. As expected, Ni films deposited on the planar PPX-C films exhibit low roughness and are essentially nonporous. In contrast, Ni films plated

onto the helical and columnar NTF templates are rougher ($\sim 4\text{--}5$ times) with moderate degrees of porosity (30–35 %), consistent with the nanostructured nature of the NTF templates. As expected, column widening and separation of the columnar NTF PPX-C filament clusters templates deposition of a somewhat rougher Ni film (i.e., $\sim 40 \text{ nm}$) than that observed for Ni films (i.e., $\sim 35 \text{ nm}$) templated by the helical NTF, at least for the plating conditions used here. However, because EL Ni film morphology is sensitive to ligand and Pd^{II} surface concentrations,^[25] as well as plating conditions,^[16] these factors offer the potential to readily control Ni roughness. For example, preliminary experiments show that helical NTFs treated for only $\sim 17 \text{ h}$ by pyridine (aq) solution provide rougher Ni films (i.e., $\sim 68 \text{ nm}$), which is consistent with this argument.

In contrast to roughness, Ni porosity is primarily influenced by the morphology of the underlying NTF template, at least for the thin Ni films considered here (see below). Similar total surface porosity values shown in Table 1 for Ni films deposited on helical (35 %) and columnar (30 %) NTFs are best understood by considering the nucleation and growth of the NTF templates. De-

position of NTFs occurs via a mechanism in which initial surface migration of vapor deposited reactive species to nucleation sites promotes growth of clusters of nested helical or columnar PPX-C filaments.^[14,15] Within a cluster, individual 50–200 nm diameter PPX-C filaments are separated from adjacent filaments by less than $\sim 20 \text{ nm}$. Adjacent clusters are separated from one another by distances of $\sim 200\text{--}400 \text{ nm}$, corresponding to the sizes of surface depletion regions in which migration has left the local concentrations of reactive species

Table 1. Characteristics of the EL Ni Films.

PPX-C film substrate [a]	Ni film RMS roughness [nm] [b]	Ni film surface porosity [%] [b]
planar [c]	9	<5
helical NTF [d]	35	35
columnar NTF [d]	40	30

[a] Type of PPX-C film used for EL Ni deposition. [b] Values calculated from AFM scans as described in the Experimental Section. [c] Substrate treated for 4 days at $(22 \pm 2) \text{ }^\circ\text{C}$ using 0.2 M pyridine (aq) solution, catalyzed for 45 min by PD1 and plated for 15 min using 10 % NIPOSIT 468B EL Ni bath. [d] Substrate treated for 48 h at $(22 \pm 2) \text{ }^\circ\text{C}$ using 0.2 M pyridine (aq) solution, catalyzed for 45 min by PD1 and plated for 15 min using 10 % NIPOSIT 468B EL Ni bath.

insufficient for new filament nucleation and growth. Consequently, templated Ni deposition on these NTFs leads to a bimodal pore distribution, as shown in Figure 3A. Larger, irregular-shaped Ni pores (Type I, > 70 % population; ~60–120 nm width) and smaller nearly circular Ni pores (Type II, < 30 % population, ~10–40 nm diameter) are observed, corresponding approximately to plated NTF templates comprising separations of PPX-C clusters and filaments, respectively. Because the larger Type I pores dominate pore surface areas in each case, similar total surface porosity values are obtained for both helical- and columnar-templated Ni films.

Precise measurements of the thickness of Ni deposited on the NTF top surface are rendered difficult by the inherent roughness of the NTF (i.e., ~40–60 nm).^[14,15] Nevertheless, focused ion-beam milling to selectively remove Ni from helical NTF regions corresponding to PPX-C filament clusters (i.e., regions associated with Type II pores in Fig. 3A), followed by SEM examination of the milled area cross-sections, yields a Ni thickness of ~50–80 nm. In comparison, Ni films of ~35–40 nm thickness are deposited on flat aminosiloxane-coated Si wafers catalyzed and plated under conditions identical to those used for our NTFs.^[26] Such differences are not unexpected, given the magnitude of the NTF surface roughness and the isotropic nature of the EL process. Specifically, the combination of perpendicular and lateral Ni growth from catalyzed PPX-C filament tips and sidewalls, respectively, at the NTF top surface leads to more rapid agglomeration and fusion of adjacent Ni nodules than for a flat surface, enhancing the apparent Ni deposition rate. Consequently, the measured Ni thickness reflects contributions from Ni deposited perpendicular to the NTF surface plane at PPX-C cluster and filament tips and Ni laterally deposited in filament interstices near the NTF surface. Ni surface roughness is simultaneously decreased (note Table 1) relative to a nonplated NTF as Ni fills the filament interstices, which supports this mechanism.

Similar difficulties are encountered in characterizing the Ni plate deep within the NTF pores, where mixed-potential theory (MPT) arguments predict thinner Ni deposits due to non-linear diffusion and concentration-depletion effects.^[9,24,27] We are currently working to acquire the necessary cross-sectional TEM (transmission electron microscopy) data to test this hypothesis and will report our results in a full-length publication later. In the interim, it is worth noting that observation of Ni deposition at greater depths (i.e., ~40 μm) inside NTFs treated by pyridine vapor than for those treated by pyridine (aq) solution (~20 μm) lends support for the presence of thinner Ni films deep within the pores, consistent with MPT predictions. It further indicates that at least some larger type I pores are likely to remain open throughout their length following Ni plating of NTFs treated by pyridine (aq) solution. In fact, in separate experiments coloration of an underlying helical NTF via diffusion of aqueous thymol blue solution through the porous Ni film coating is observed, confirming the open nature of the pores in our Ni membranes.

In conclusion, we have illustrated here a simple method for conformal EL Ni deposition that permits control of Ni mor-

phology and topology via use of tailored nanostructured PPX-C thin-polymer-film templates. The metallization process is well described using a model adapted from previous work^[17] and relies on noncovalent adsorption of metal-binding ligand to NTFs to covalently anchor the Pd^{II} catalyst required for EL Ni deposition. Consequently, direct chemical modification of PPX-C leading to potential degradation of its biocompatible surface is avoided while maintaining Ni adhesion and control of the metal/polymer interface. Although we have utilized Ni films in this example, the fabrication of films of other metals, oxides, and biomolecules by electroless, CVD, or direct-binding methods^[13,28,29] is clearly possible, provided that suitable “ligand” adsorbates are available to template material deposition. We are currently investigating these prospects further with the aim of extending our process to include materials useful for biomedical implantation, metal–dielectric composites, energy storage, SERS platform, and related applications.

Experimental

Materials: All chemicals were A.C.S. reagent grade and were used as received from Aldrich Chemical Co. unless otherwise noted. Nitrogen gas was from liquid N₂ boil-off and H₂O was deionized (18 M Ω cm resistivity; Barnstead Nanopure II deionizer). Native oxide *n*-type <100> Si wafers were from Wafernet Inc. PPX-C planar films and NTFs were prepared from dichloro-[2.2]paracyclophane (DCPC; a.k.a. dichloro-*di-p*-xylylene or Parylene Type C; Lot #060514; Parylene Distribution Services Inc.) on native oxide Si wafers using the procedure and instrument described previously [14,15]. Each film was deposited using ~0.7 g DCPC at vaporizer and pyrolysis temperatures of 175 °C and 690 °C, respectively. The flux deposition angle (α), film growth angle (β) and turntable rotation rate (ω) for the helical and columnar NTFs used here are shown in Figure 1. PD1 electroless Pd^{II} catalyst dispersion was prepared from Na₂Cl₄·3H₂O (Strem Inc.), morpholinoethane sulfonic acid, and NaCl according to the procedure described in an earlier paper [23]. The NIPOSIT 468B EL Ni bath from Rohm & Haas (Shipley Co.) was prepared according to the manufacturer's instructions; the bath was diluted to 10 % strength with H₂O prior to use.

General Procedures: All work was performed in a well-ventilated fume hood. Samples of PPX-C films (either planar or nanostructured) were immersed in (solution deposition) or suspended over (vapor deposition) freshly prepared 0.1–0.2 M pyridine (aq) solution at (22±2) °C for ~40–48 h in a tightly sealed glass jar to adsorb pyridine ligand onto the film surface. Samples were then removed from jar, rinsed three times in H₂O, and dried in a stream of filtered N₂ gas. Samples were then treated with PD1 catalyst for ~45 min. Excess PD1 catalyst was carefully removed from the sample surface by Pasteur pipet. The samples were then gently rinsed two times in H₂O and immediately immersed in the EL Ni bath for ~15–20 min at (22±2) °C for plating. The samples were occasionally agitated gently to remove any bubbles of hydrogen gas adhering to the surface. Following plating, samples were rinsed two times in H₂O, dried in a stream of filtered N₂ gas, and visually inspected to ascertain the degree of metallization, if any. Dried plated samples were stored in Fluoroware containers until needed for characterization. Ni porosity was confirmed as follows: A Ni-coated helical NTF on a Si wafer was placed on a flat surface and a ~10 μL droplet of 1.0 M thymol blue dye (aq) solution was applied to the center of the Ni film. An inverted beaker was placed over the sample to minimize evaporation of the droplet and the system was allowed to stand undisturbed for ~3 h. The droplet was then carefully removed from the Ni surface using a microsyringe and the sample was

allowed to air dry for ~30 min. The Ni-coated NTF was then carefully peeled from the Si-wafer support and examined for the presence of dye coloration of the underlying white NTF due to dye diffusion through the Ni film.

Characterization: X-ray photoelectron spectroscopy (XPS) data were acquired using an Axis Ultra XPS system (Kratos) with a monochromatic Al K α X-ray source, 20 eV pass energy (700 $\mu\text{m} \times 300 \mu\text{m}$ hybrid sample spot size), and 90° take-off angle under high-vacuum conditions (10⁻⁹ Torr, 1 Torr = 133.322 N m⁻¹). All spectra were referenced to the C 1s peak at 284.6 eV and analyzed using the CasaXPS v. 2.1.9 program supplied by the manufacturer. Spectra were corrected for variations in detector sensitivity between elements to estimate surface abundance (at %) using instrument correction factors supplied by the manufacturer and literature procedures [30]. Ni-film morphology was characterized using a scanning electron microscope (XL-30, Philips), as well as an atomic force microscope (Nanoscope E, Veeco Inc.) equipped with an air chamber and silicon nitride cantilevers operating in contact mode. Surface roughness of bare and Ni-plated NTFs was also calculated from the AFM measurements after image-data correction to account for sample tilt and application of a median filter. For porous Ni samples, pore densities, distributions, and diameters were estimated by projecting the AFM image onto the *xy* plane using data acquired from five randomly selected 2 $\mu\text{m} \times 2 \mu\text{m}$ scanned regions on each sample. Surface porosity was calculated by analyzing the bearing curve of the AFM image at its inflection point. The cross-sectional structure of and penetration of the Ni into the NTFs was probed (10⁻⁷ Torr) using the energy dispersive X-ray (EDAX) attachment (Ametex) of the SEM. For Ni thickness measurements, a focused ion beam (FEI Quanta 200 3D, OR) of Ga⁺ was impinged on the Ni-templated NTF surface with 30 kV kinetic energy to remove Ni from the surface, followed by observation and measurement of the Ni cross-section thickness using a field-emission SEM (JEOL 6700F, Japan).

Received: May 3, 2007
Revised: August 2, 2007

- [1] A. J. Smith, D. L. Trimm, *Annu. Rev. Mater. Res.* **2005**, *35*, 127.
- [2] C. W. Chao, Y. C. S. Wu, G.-R. Hu, M.-S. Feng, *J. Electrochem. Soc.* **2003**, *150*, C631.
- [3] L.-S. Zhang, W. Wang, Z.-Y. Li, *J. Inorg. Mater.* **2006**, *21*, 1103.
- [4] K. Yuasa, M. Ikoma, *Res. Chem. Intermed.* **2006**, *32*, 461.
- [5] S. M. Williams, A. D. Stafford, K. R. Rodriguez, T. M. Rogers, J. V. Coe, *J. Phys. Chem. B* **2003**, *107*, 11871.
- [6] I. Lee, P. T. Hammond, M. F. Rubner, *Chem. Mater.* **2003**, *15*, 4583.
- [7] B.-H. Chen, L. Hong, Y. Ma, T.-M. Ko, *Ind. Eng. Chem. Res.* **2002**, *41*, 2668.
- [8] C.-C. Lee, T.-S. Chou, *Ind. Eng. Chem. Res.* **1998**, *37*, 1815.
- [9] A. M. T. Vanderputten, J. W. G. Debakker, *J. Electrochem. Soc.* **1993**, *140*, 2229.
- [10] X. Zhang, K.-N. Tu, *J. Am. Chem. Soc.* **2006**, *128*, 15036.
- [11] D. Ishii, T. Nagashima, M. Udatsu, R.-D. Sun, Y. Ishikawa, S. Kawasaki, M. Yamada, T. Iyoda, M. Nakagawa, *Chem. Mater.* **2006**, *18*, 2152.
- [12] M. Knez, A. M. Bittner, F. Boes, C. Wege, H. Jeske, E. Mai, K. Kern, *Nano Lett.* **2003**, *3*, 1079.
- [13] R. R. Price, W. J. Dressick, A. Singh, *J. Am. Chem. Soc.* **2003**, *125*, 11259.
- [14] M. C. Demirel, E. So, T. M. Ritty, S. H. Naidu, A. Lakhtakia, *J. Biomed. Mater. Res., Part B* **2007**, *81B*, 219.
- [15] M. Cetinkaya, S. Boduroglu, M. C. Demirel, *Polymer* **2007**, *48*, 4130.
- [16] G. O. Mallory, in *Electroless Plating: Fundamentals & Applications* (Eds: G. O. Mallory, J. B. Hajdu), American Electroplaters and Surface Finishers Society, Orlando, FL **1990**, Ch. 1.
- [17] M.-S. Chen, S. L. Brandow, T. L. Schull, D. B. Chrisey, W. J. Dressick, *Adv. Funct. Mater.* **2005**, *15*, 1364.
- [18] S. L. Brandow, T. L. Schull, B. D. Martin, D. C. Guerin, W. J. Dressick, *Chem. Eur. J.* **2002**, *8*, 5363.
- [19] W. J. Dressick, M.-S. Chen, S. L. Brandow, K. W. Rhee, L. M. Shirey, F. K. Perkins, *Appl. Phys. Lett.* **2001**, *78*, 676.
- [20] B. D. Martin, S. L. Brandow, W. J. Dressick, T. L. Schull, *Langmuir* **2000**, *16*, 9944.
- [21] W. J. Dressick, M.-S. Chen, S. L. Brandow, *J. Am. Chem. Soc.* **2000**, *122*, 982.
- [22] W. J. Dressick, C. S. Dulcey, J. H. Georger, Jr., G. S. Calabrese, J. M. Calvert, *J. Electrochem. Soc.* **1994**, *141*, 210.
- [23] W. J. Dressick, L. M. Kondracki, M.-S. Chen, S. L. Brandow, E. Matijević, J. M. Calvert, *Colloids Surf., A* **1996**, *108*, 101.
- [24] M.-S. Chen, S. L. Brandow, C. S. Dulcey, W. J. Dressick, G. N. Taylor, J. F. Bohland, J. H. Georger, Jr., E. K. Pavelchek, J. M. Calvert, *J. Electrochem. Soc.* **1999**, *146*, 1421.
- [25] S. L. Brandow, W. J. Dressick, C. R. K. Marrian, G.-M. Chow, J. M. Calvert, *J. Electrochem. Soc.* **1995**, *142*, 2233.
- [26] D. I. Ma, L. Shirey, D. McCarthy, A. Thompson, S. B. Qadri, W. J. Dressick, M.-S. Chen, J. M. Calvert, R. Kapur, S. L. Brandow, *Chem. Mater.* **2002**, *14*, 4586.
- [27] I. Ohno, *Mater. Sci. Eng., A* **1991**, *146*, 33.
- [28] K. Koumoto, S. Seo, T. Sugiyama, W. S. Seo, W. J. Dressick, *Chem. Mater.* **1999**, *11*, 2305.
- [29] S. J. Potochnik, P. E. Pehrsson, D. S. Y. Hsu, J. M. Calvert, *Langmuir* **1995**, *11*, 1841.
- [30] J. F. Moulder, W. F. Stickle, P. E. Sobol, K. D. Bomben, in *Handbook of X-ray Photoelectron Spectroscopy* (Eds: J. Chastain, R. C. King, Jr.), Physical Electronics Inc., Eden Prairie, MN **1995**, p. 25.